PROCEEDINGS OF SCIENCE

Towards the First Neutrino Search with RNO-G

The RNO-G Collaboration
(a complete list of authors can be found at the end of the proceedings)

E-mail: avijai@umd.edu, baclark@umd.edu

The Radio Neutrino Observatory in Greenland (RNO-G) is located at Summit Station and is designed to detect Askaryan emission from ultra-high energy (UHE) neutrinos above 100 PeV. The detector is proposed to have 35 stations of which 8 have been deployed so far. Each station is made up of 9 antennas at the surface and 18 antennas that are buried in the ice down to a depth of 100 meters with the purpose of triggering on and reconstructing neutrino-like signals. The partially completed detector has been collecting data since 2021 and this data is being used for RNO-G's first neutrino search. This talk will outline progress towards this search, such as the data processing pipeline, analysis variables, initial reconstructions, and background/signal separation.

Corresponding authors: Aishwarya Vijai[1], Brian Clark[1*]
[1] *University of Maryland, College Park*
[*] Presenter

39th International Cosmic Ray Conference (ICRC2025)
15–24 July 2025
Geneva, Switzerland

PoS(ICRC2025)1204

1. Introduction

The Radio Neutrino Observatory in Greenland (RNO-G) is located at Summit Station and aims to find ultra-high energy (> 100 PeV) neutrinos via the radio detection method [1, 2]. The detection mechanism relies on the Askaryan effect [3] which arises when UHE neutrinos interact with ice and the produced particles generate a broadband (0.1-1 GHz) radio pulse. RNO-G aims to detect UHE neutrinos through these radio wave byproducts. The detector is proposed to have 35 stations spaced approximately 1.25 km apart as shown in Figure 1.

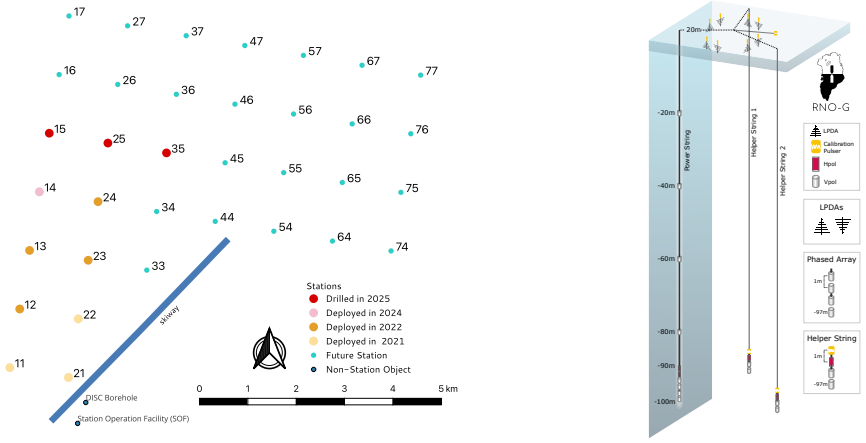

(a) The planned 35 station RNO-G array layout **(b)** The layout of a single RNO-G station

Figure 1: (Left) RNO-G 35 Station Array with currently deployed (orange) and future (blue) stations. (Right) A single station of RNO-G with 3 strings/cables carrying antennas.

Currently, eight stations have been installed. Each station contains three vertical cables ("strings") carrying antennas embedded in ice. The strings are of two types: power and helper. The power string is the primary string responsible for triggering on neutrino events while the helper strings are used for neutrino event reconstruction (identifying neutrino energy/direction) and calibration. The antennas attached to these strings are of 4 types as shown in 1b. HPols capture the horizontal polarization of an incoming signal. VPols capture the vertical polarization. Calibration pulsers emit pulses for testing purposes and the LPDAs (Log Periodic Dipole Antennas) are surface antennas used to distinguish between signals going up through and down through the detector. Signals captured by these antennas are transmitted via the strings to the digitizer, which reads out the signal in blocks of 128 samples. These digitizers are run at 2.4 or 3.2 gigasamples per second. The readout window is made of 2048 samples (one trace), corresponding to ~853 nanoseconds (ns).

2. Data Processing Pipeline

The partially completed RNO-G detector has been collecting data since 2021. This data is being used for RNO-G's first neutrino search. Firstly, several cuts are applied to this data in order to a create a "good run list" i.e. a dataset that can be used for the neutrino search. These cuts exclude runs that are not classified as "Physics" runs, such as runs used for calibration purposes. In addition, runs with a high trigger rate are excluded as they are usually composed of anthropogenic noise. Additional cuts are made in order to remove runs with a high root mean square (RMS) noise.

For each antenna ("channel"), the average RMS noise of the run is obtained. The runs are grouped by year and an empirical cumulative distribution function (ECDF) is obtained for each year and channel. This ECDF is fit to the ECDF of a normal distribution to identify fit parameters (mean μ and standard deviation σ). A cut at 6σ is applied to remove runs with a significant deviation in RMS noise from μ. These cuts collectively remove approximately 1.4 % of the total data collected.

The good runs are then passed through several stages of filtering and processing. The first step removes glitches. A glitch is a part of a trace in which a single sample deviates by a large amount compared to the samples surrounding it due to a scrambling of the order of readout blocks. This occurs due to occasional problems with the digitizer. If a glitch is found in a trace, the entire trace is removed. After glitch removal, the good runs undergo block offset filtering which handles block offsets i.e. deviations from zero of the average voltage in a block as read out by the digitizer (see Section 1). To preserve uniformity across all 16 blocks of a single trace, block offsets from zero must be corrected for. The offset is fitted for and then subtracted. Lastly, delays i.e. time delays caused by the cables carrying the antennas and the readout chain, are subtracted. All of these steps are encompassed in a single module within NuRadioMC [4], the software package used by RNO-G.

Additional processing is housed in a separate module within NuRadioMC. This module first upsamples the data to 5GHz to allow for better detection of the maximum signal amplitude and timing. A bandpass filter between 100 and 600 MHz is then applied, corresponding to the frequency band within which the RNO-G in-ice antennas are most sensitive. After this, the data is dedispersed to remove the dispersion caused by the signal chain. Finally, a continuous waveform (CW) emission filter is applied. CW emission is high-amplitude signals of anthropogenic origin that are concentrated at a few frequencies. The CW filter uses a method called sine wave subtraction in which a sine wave corresponding to the peak of the CW emission is constructed and subtracted from the original waveform. This method removes CW emission at the frequency corresponding to the sine wave, leaving surrounding frequencies of the signal intact. Comparing this with the more well known notch filter, a notch filter removes all the power at a particular frequency while sine wave subtraction removes just the sine wave component at that frequency. Thus, a notch filter is more "unphysical" and a CW sine wave subtraction filter is used instead.

3. Analysis Variables

After the data has been cleaned, higher level physics variables are calculated for each event in a run. These variables will be explored in this section.

The first analysis variables calculated are the signal to noise ratio (SNR) and the root power ratio (RPR) in order to identify impulsive events. The SNR is defined as the ratio between the peak to peak voltage (difference between the maximum and minimum voltage in a trace) and the RMS noise. Impulse neutrino-like signals are expected to stand out above background noise i.e. have a high SNR. The RPR is the ratio of the power of the trace to the RMS noise. Just like the SNR, we expect neutrino-like signals to have a high RPR.

After calculating the average SNR and RPR for each event as seen across all in-ice antennas, the event is reconstructed. The purpose of interferometric reconstruction is to determine the vertex location of an event using RNO-G's array of antennas. The procedure can be broken down into 4 steps. Firstly, travel time maps are generated. The travel time is defined as the time taken to travel from a potential source location to an antenna. This travel time accounts for signal propagation

through the various layers of ice in Greenland and the transition from ice to air at the surface. Depth-dependent refractive indices are used to solve the Eikonal equation at each potential source location. The Eikonal equation [5] connects the travel time to the refractive index through $|\nabla T| = \frac{n(z)}{c}$ where c is the speed of light in vacuum in m/s, n is the refractive index as a function of depth (z) and ∇T is the spatial gradient of the travel time in units of s/m. This equation can be solved using Python's Pykonal package [6].

Secondly, the correlation is obtained as a function of lag for the Hilbert envelope of the event traces. The Hilbert envelope is made by converting the real trace to a complex ("analytic") signal via a Fourier transform. The envelope is smoother in cases where there is a lot of noise in the original trace. Thus, it is better for reconstruction purposes. The correlation quantifies the similarity between a pair of these Hilbert envelopes. It is calculated by shifting the envelope as seen in one antenna by a lag, multiplying the overlapping values between envelopes, and summing over them as shown in Equation 1.

$$\sum_{i=0}^{i=n} \frac{x(i)y(i-k)}{N_k} \tag{1}$$

Where k is the lag and n is the number of samples in the envelopes (x,y). This sum is calculated for multiple lags and divided by the number of overlapping values (N_k) between the two envelopes at each lag (k). As seen in Equation 1, the correlation value diverges at the edge of the region of support as the number of overlapping samples N_k becomes small. To avoid this, a Hanning window [7] is applied to taper the edges of the correlation function to zero.

Given the travel time map for each antenna, lags can be calculated for each antenna pair as the difference in the travel time between them (delay time). For each delay time, the corresponding correlation can be found at each potential source location using the correlation function described above. These correlation values are then summed over all antenna pairs to obtain a single correlation value for each potential source location. Figure 2b shows the correlation map for a pulse emitted by the calibration pulser. The blue star denotes the location of the pulser, which aligns with the azimuth and elevation corresponding to the maximum correlation value. This maximum correlation value and its corresponding source location is stored for each event.

Post reconstruction, the surface correlation ratio (SCR) is calculated in order to determine if the event originates from the surface or within the ice. Neutrino interactions are in-ice events and thus the SCR, alongside other analysis variables, can be used to identify them. The SCR is defined as the ratio between the maximum correlation among potential source locations within a +/- 10 meter band around the surface (boundary between air and ice) and the maximum correlation across all potential source locations. For each event, the SCR, the maximum surface correlation value and the location corresponding to the maximum surface correlation value is stored.

Lastly, the coherently summed waveform (CSW) is made for each event by shifting traces by a lag corresponding to the maximum correlation between a pair of traces. This correlation is found within a small window around the lag corresponding to the maximum reconstructed correlation value. The shifted traces are then summed to create the CSW. The SNR, RPR, peak, power and impulsivity of the CSW is extracted. The impulsivity quantifies how sharply peaked the CSW is and is calculated by the formula $2 * \frac{\sum(CDF)}{n} - 1$ where CDF stands for the cumulative distribution function and n is the length of the CDF [8]. To find the CDF, the absolute value of the trace is firstly sorted from smallest to largest. For each value in the sorted trace, the fraction of values less

than or equal to that value is given by the CDF. The mean of the CDF is lower for a spikier signal as most values in the trace are near zero and only a few are large. By multiplying the mean of the CDF by 2 and subtracting 1, the impulsivity is normalized to be between 0 and 1 with impulsivity > 0.5 indicating a more "impulse-like" CSW.

The CSW has a higher SNR compared to the individual signals seen in each channel as shown in Figure 2a. Thus, the CSW helps identify low SNR i.e. weaker neutrino-like signals.

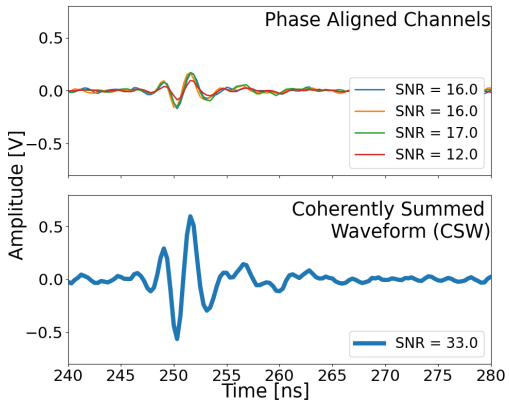

(a) The SNR comparison between CSW and individual channels

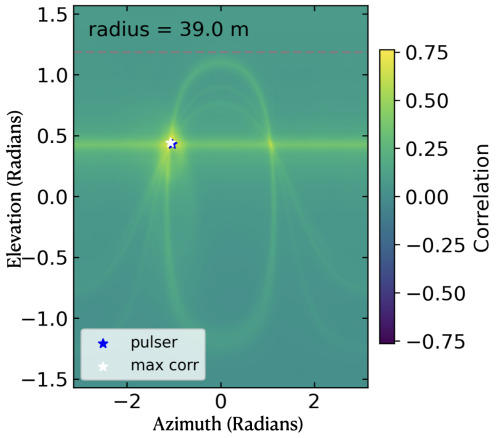

(b) The correlation map of a calibration pulse

Figure 2

4. Initial Reconstructions

In order to test the interferometric reconstruction, calibration pulses and simulated neutrino signals were reconstructed and the position associated with their maximum correlation values were compared to their actual positions.

Calibration pulses are impulsive signals emitted by a single antenna on the helper string. Approximately 300 calibration pulses were reconstructed for testing. Figures 3b and 3a compare the actual and reconstructed elevation (θ) and azimuth (ϕ) of these calibration pulses.

As seen in Figures 3a and 3b, the actual position marked by the gray dashed line agrees within 1 degree with both distributions. The reconstruction resolution is 0.1 degrees in ϕ and 0.9 degrees in θ as quantified by the gaussian fits shown.

A similar test was done for simulated neutrinos. Electron neutrinos were simulated together with noise at an energy of 10^{18} eV, undergoing neutral current interactions. Figures 3c and 3d shows a histogram of the difference between the actual and reconstructed θ and ϕ of these simulated neutrinos. Only neutrinos that used a direct ray tracing solution are shown because the interferometric reconstruction currently only uses direct ray tracing. Reflected and refracted ray tracing will be included soon.

The simulated neutrino distribution is centered at 0 degrees for ϕ and -1.5 degrees for θ, with a σ of approximately 1 degree for both distributions. This is comparable to other radio-based neutrino detectors like ARA [9] and ARIANNA [10]. The outliers in these plots correspond to weak neutrino signals dominated by background noise.

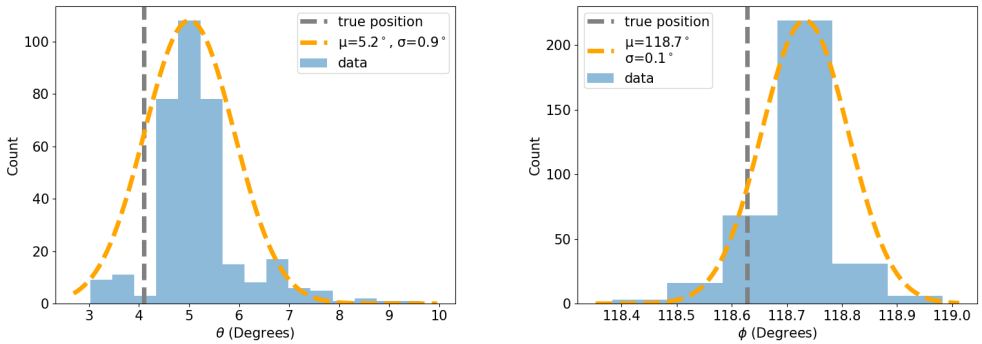

(a) The distribution of the reconstructed elevation of calibration pulses

(b) The distribution of the reconstructed azimuth of calibration pulses

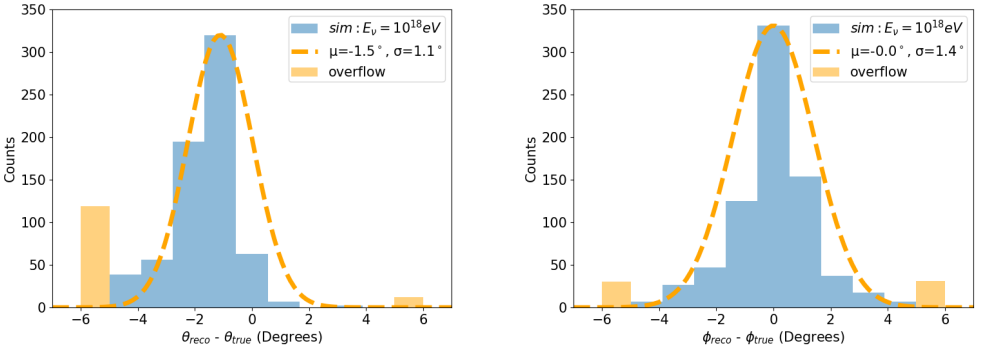

(c) The distribution of the reconstructed elevation of simulated neutrinos

(d) The distribution of the reconstructed azimuth of simulated neutrinos

Figure 3: The distributions of reconstructed arrival directions for calibration pulses and simulated neutrinos

5. Results

After testing the reconstruction, the analysis variables were calculated for all events from the good run list in 2021 for station 11. Figure 4a shows a 2D histogram of the surface correlation ratio as a function of elevation for data (blue) and for simulated neutrinos (red). This plot was used to qualitatively create a cut in elevation and surface correlation ratio that minimized surface backgrounds while saving the majority of neutrinos. The cut is shown in Figure 4a as a black box with boundaries at an elevation of 0.25 radians and a surface correlation ratio of 0.6. These cuts were determined qualitatively and will be optimized in the future. This cut was applied to 2021 data and Figure 4b was made post-cut. Figure 4b shows a 2D histogram of the maximum correlation as a function of the CSW SNR for data (blue) and simulated neutrinos (red). A clear separation can be seen between simulated neutrinos and data, with data clustering at low SNR and low maximum correlation. Thus, the maximum correlation and CSW SNR, alongside other analysis variables, can be used to separate data which is primarily composed of background noise, from neutrino-like signals.

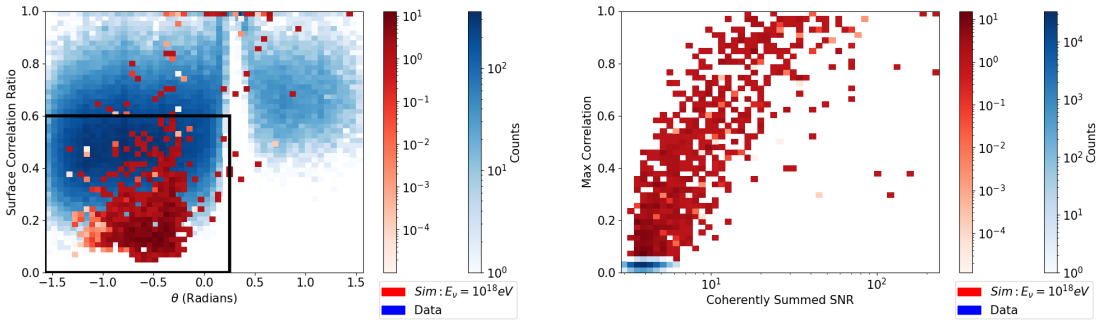

(a) A 2D histogram of surface correlation ratio as a function of zenith

(b) A 2D histogram of maximum correlation value as a function of CSW SNR

Figure 4

6. Background and Signal Separation

Once all the 2021 data was processed for station 11, a linear discriminant analysis (LDA) [11] was developed to separate noise from neutrino-like signals as was done in ARA. The LDA currently uses all the analysis variables listed in Section 3 and will be optimized, including the addition of more variables. The LDA develops a single variable (linear discriminant) for each event that is defined by a combination of the analysis variables to maximize the separation between noise and neutrino-like signal distributions. Neutrino-like signal distributions are simulated as described in Section 4. The LDA maximizes the separation between this simulated neutrino distribution and the 2021 processed data (noise) as shown in Figure 5. The 2021 processed data is considered to be primarily noise, based on the separation between data and simulated neutrino distributions shown in Figures 4a and 4b.

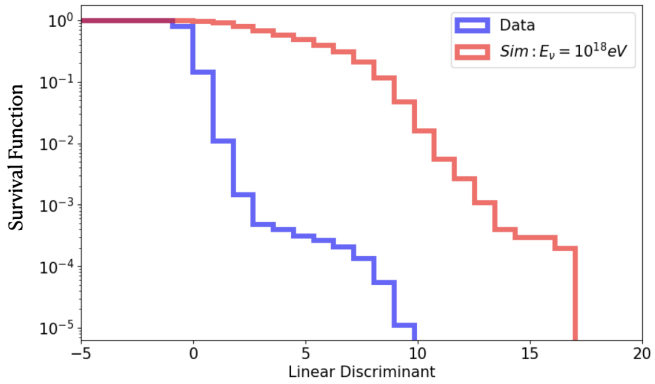

Figure 5: The LDA Projection of data and simulated neutrino distributions

Figure 5 contains the survival functions for the data (blue) and simulated neutrino (red) distributions as a function of the linear discriminant developed by the LDA. The survival function gives the probability of an event passing a cut at a particular value for the linear discriminant. By eye it is clear that a linear discriminant value of approximately 3 would remove most of the noise (data) and preserve neutrinos. The determination of a precise cut to separate the two distributions is ongoing work.

7. Conclusion

These proceedings outline progress that has been made towards RNO-G's first neutrino search. A data processing pipeline has been set up and analysis variables have been calculated for processed data taken by Station 11 in the year 2021. Neutrinos have also been simulated at an energy of 10^{18} eV and those that utilize a direct ray tracing solution were used to test the interferometric reconstruction and train an LDA. The LDA maximizes separation between data and simulated neutrinos and will be used to create a cut between these distributions. In the future, the analysis will be applied to additional stations and years of data to set a limit on the diffuse neutrino flux.

References

[1] **RNO-G** Collaboration, J.A.Aguilar *et al. JINST* **16** (10, 2020) P03025.

[2] **RNO-G** Collaboration, S. Agarwal *et al. JINST* **20** no. 04, (2025) P04015.

[3] G. Askar'yan, "Excess negative charge of an electron-photon shower and its coherent radio emission." https://inspirehep.net/literature/1351286, 02, 1962.

[4] C. Glaser and other *European Physical Journal* (06, 2019) .

[5] M. Slawinski, *Handbook of Geophysical Exploration: Seismic Exploration, Chapter 8: Hamilton's ray equations*, vol. 34. Pergamon, 2003.

[6] M. C. White and other *Seismological Research Letters* (2020) .

[7] "scipy.signal.windows.hann." https://docs.scipy.org/doc/scipy/reference/generated/scipy.signal.windows.hann.html.

[8] **ANITA** Collaboration, P. Gorham *et al. Physical Review D* **98** no. 02, (2018) 022001.

[9] **ARA** Collaboration, P. Allison *et al.*, "Design and Initial Performance of the Askaryan Radio Array Prototype EeV Neutrino Detector at the South Pole," 05, 2011.

[10] **ARIANNA** Collaboration, S. Barwick *et al.*, "A first search for cosmogenic neutrinos with the arianna hexagonal radio array," 10, 2014.

[11] "Linear discriminant analysis." https://scikit-learn.org/stable/modules/generated/sklearn.discriminant_analysis.LinearDiscriminantAnalysis.html.

PoS(ICRC2025)1204

Full Author List: RNO-G (June 30th, 2025)

S. Agarwal[1], J. A. Aguilar[2], N. Alden[3], S. Ali[1], P. Allison[4], M. Betts[5], D. Besson[1], A. Bishop[6], O. Botner[7], S. Bouma[8], S. Buitink[9,10], R. Camphyn[2], J. Chan[6], S. Chiche[2], B. A. Clark[11], A. Coleman[7], K. Couberly[1], S. de Kockere[12], K. D. de Vries[12], C. Deaconu[3], P. Giri[13], C. Glaser[7], T. Glüsenkamp[7], H. Gui[4], A. Hallgren[7], S. Hallmann[14,8], J. C. Hanson[15], K. Helbing[16], B. Hendricks[5], J. Henrichs[14,8], N. Heyer[7], C. Hornhuber[1], E. Huesca Santiago[14], K. Hughes[4], A. Jaitly[14,8], T. Karg[14], A. Karle[6], J. L. Kelley[6], C. Kopper[8], M. Korntheuer[2,12], M. Kowalski[14,17], I. Kravchenko[13], R. Krebs[5], M. Kugelmeier[6], R. Lahmann[8], C.-H. Liu[13], M. J. Marsee[18], K. Mulrey[10], M. Muzio[6,5], A. Nelles[14,8], A. Novikov[19], A. Nozdrina[4], E. Oberla[3], B. Oeyen[20], N. Punsuebsay[19], L. Pyras[14,21], M. Ravn[7], A. Rifaie[16], D. Ryckbosch[20], F. Schlüter[2], O. Scholten[12,22], D. Seckel[19], M. F. H. Seikh[1], Z. S. Selcuk[14,8], J. Stachurska[20], J. Stoffels[12], S. Toscano[2], D. Tosi[6], J. Tutt[5], D. J. Van Den Broeck[12,9], N. van Eijndhoven[12], A. G. Vieregg[3], A. Vijai[11], C. Welling[3], D. R. Williams[18], P. Windischhofer[3], S. Wissel[5], R. Young[1], A. Zink[8]

[1] University of Kansas, Dept. of Physics and Astronomy, Lawrence, KS 66045, USA
[2] Université Libre de Bruxelles, Science Faculty CP230, B-1050 Brussels, Belgium
[3] Dept. of Physics, Dept. of Astronomy & Astrophysics, Enrico Fermi Inst., Kavli Inst. for Cosmological Physics, University of Chicago, Chicago, IL 60637, USA
[4] Dept. of Physics, Center for Cosmology and AstroParticle Physics, Ohio State University, Columbus, OH 43210, USA
[5] Dept. of Physics, Dept. of Astronomy & Astrophysics, Center for Multimessenger Astrophysics, Institute of Gravitation and the Cosmos, Pennsylvania State University, University Park, PA 16802, USA
[6] Wisconsin IceCube Particle Astrophysics Center (WIPAC) and Dept. of Physics, University of Wisconsin-Madison, Madison, WI 53703, USA
[7] Uppsala University, Dept. of Physics and Astronomy, Uppsala, SE-752 37, Sweden
[8] Erlangen Centre for Astroparticle Physics (ECAP), Friedrich-Alexander-University Erlangen-Nürnberg, 91058 Erlangen, Germany
[9] Vrije Universiteit Brussel, Astrophysical Institute, Pleinlaan 2, 1050 Brussels, Belgium
[10] Dept. of Astrophysics/IMAPP, Radboud University, PO Box 9010, 6500 GL, The Netherlands
[11] Department of Physics, University of Maryland, College Park, MD 20742, USA
[12] Vrije Universiteit Brussel, Dienst ELEM, B-1050 Brussels, Belgium
[13] Dept. of Physics and Astronomy, Univ. of Nebraska-Lincoln, NE, 68588, USA
[14] Deutsches Elektronen-Synchrotron DESY, Platanenallee 6, 15738 Zeuthen, Germany
[15] Whittier College, Whittier, CA 90602, USA
[16] Dept. of Physics, University of Wuppertal D-42119 Wuppertal, Germany
[17] Institut für Physik, Humboldt-Universität zu Berlin, 12489 Berlin, Germany
[18] Dept. of Physics and Astronomy, University of Alabama, Tuscaloosa, AL 35487, USA
[19] Dept. of Physics and Astronomy, University of Delaware, Newark, DE 19716, USA
[20] Ghent University, Dept. of Physics and Astronomy, B-9000 Gent, Belgium
[21] Department of Physics and Astronomy, University of Utah, Salt Lake City, UT 84112, USA
[22] Kapteyn Institute, University of Groningen, PO Box 800, 9700 AV, The Netherlands

Acknowledgments

We are thankful to the support staff at Summit Station for making RNO-G possible. We also acknowledge our colleagues from the British Antarctic Survey for building and operating the BigRAID drill for our project.

We would like to acknowledge our home institutions and funding agencies for supporting the RNO-G work; in particular the Belgian Funds for Scientific Research (FRS-FNRS and FWO) and the FWO programme for International Research Infrastructure (IRI), the National Science Foundation (NSF Award IDs 2112352, 2111232, 2111410, 2411590, and collaborative awards 2310122 through 2310129), and the IceCube EPSCoR Initiative (Award ID 2019597), the Helmholtz Association, the Swedish Research Council (VR, Grant 2021-05449 and 2021-00158), the University of Chicago Research Computing Center, and the European Union under the European Unions Horizon 2020 research and innovation programme (grant agreements No 805486), as well as (ERC, Pro-RNO-G No 101115122 and NuRadioOpt No 101116890).